IN SITU DIAGNOSTICS OF NANOMATERIAL SYNTHESIS BY LASER ABLATION: TIME-RESOLVED PHOTOLUMINESCENCE SPECTRA AND IMAGING OF GAS-SUSPENDED NANOPARTICLES DEPOSITED FOR THIN FILMS

D. B. GEOHEGAN*, A. A. PURETZKY*, A. MELDRUM*, G. DUSCHER**, and S. J. PENNYCOOK*
*Solid State Division, Oak Ridge National Laboratory, Oak Ridge, TN 37831-6056 odg@ornl.gov
** MPI für Metallforschung, Institut für Werkstoffwissenschaft, Seestr. 92, D-70174 Stuttgart

ABSTRACT

The dynamics of nanoparticle formation by laser ablation into background gases are revealed by gated-ICCD photography of photoluminescence (PL) and Rayleigh-scattering (RS) from gas-suspended nanoparticles. These techniques, along with gated-spectroscopy of PL from isolated, gas-suspended nanoparticles, permit fundamental investigations of nanomaterial growth, doping, and luminescence properties *prior to deposition* for thin films. Using the time-resolved diagnostics, particles unambiguously formed in the gas phase were collected on TEM grids. Silicon nanoparticles, 1–10 nm in diameter, were deposited following laser ablation into 1–10 Torr Ar or He. Three *in situ* PL bands (1.8, 2.6, 3.2 eV) similar to oxidized porous silicon were measured, but with a pronounced vibronic structure. Structureless photoluminescence bands were reproduced in the films (2.1, 2.7, 3.2 eV) only after standared annealing. The ablation of metal zinc into Ar/O_2 is also reported for the preparation of < 10 nm diameter hexagonal zincite nanocrystals, The particles were analyzed by bright field and Z-contrast TEM and high resolution EELS.

INTRODUCTION

Films incorporating silicon nanoparticles are among the most promising optoelectronic materials for applications requiring room-temperature photoluminescence and compatibility with existing silicon processing technology. These 1–10 nm-diameter particles are highly desirable light-emitting materials since quantum confinement (QC) of electron-hole pairs within a nanoparticle can result in bright luminescence from new or previously forbidden optical transitions.[1] Porous silicon (*P*-Si) luminescence is an example of this effect, in which the near-infrared emission from nanometer-sized quantum wires of crystalline Si (*c*-Si) has been traced to QC in quantum dots, i.e. particles of nanocrystalline silicon (*nc*-Si).[2] Thin films containing photoluminescent *nc*-Si and silicon-rich silicon oxide (SRSO) nanoparticles have recently been synthesized by laser ablation[3-7] in variations of the pulsed laser deposition (PLD) technique.[8] Electroluminescent light-emitting diodes (LED's) have now been fabricated from laser ablation-produced *nc*-Si films[9] and surface-emitting LED's based on oxidized *P*-Si have already been successfully integrated into microelectronic circuits.[10]

Controllable gas-phase synthesis of nanocrystals, nanotubes, and nanowires by laser ablation of solid targets into background gases has been hampered by a lack of knowledge of the spatial and temporal scales for clustering and nanoparticle growth. Until recently very little was known of these dynamics, or how the nanoparticles are transported and deposited after their formation. It is often unclear whether nanoparticles found on substrates were grown in the gas phase or from nuclei formed on the substrate surface.[5-7] Only a few *in situ* measurements of gas-formed nanoparticles have recently been employed using different techniques.[3,5-7,11-13] and considerable controversy still exists regarding the time-scales and dynamics for initial cluster formation, the establishment of critical nuclei, and nanoparticle growth in expanding laser ablation plumes (into vacuum or into background gases).

Here the synthesis and properties of silicon and zinc oxide nanoparticles formed by laser ablation are directly visualized *in situ* with a comparison of measurements involving Rayleigh-scattering (RS) and laser-induced photouminescence (PL) and *ex situ* with a combination of bright-field and Z-contrast transmission electron microscopy (TEM), electron diffraction, and high resolution electron energy loss spectroscopy (HREELS) analysis of individual nanoparticles,[12,13] These techniques form a powerful ensemble to understand nanoparticle formation and doping in gas-phase methods such as laser ablation. Rapid feedback should permit desired PL characteristics to be rapidly surveyed and optimized during synthesis, *prior to deposition.*

Mat. Res. Soc. Symp. Proc. Vol. 536 © 1999 Materials Research Society

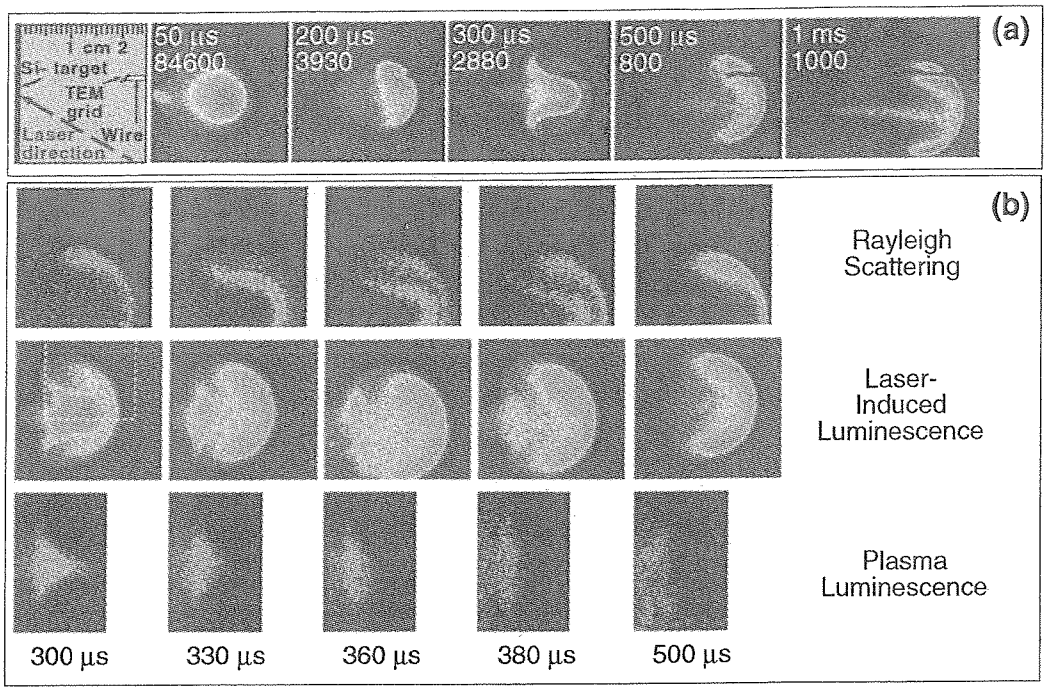

Fig. 1 - (a) Gated-intensified CCD-array (ICCD) photographs of laser-induced luminescence from clusters and nanoparticles as they form and grow following KrF-laser ablation of silicon into 10-Torr He. Photoluminescence from nanoparticles is induced and photographed (3-µs exposures) 50-ns after firing an XeCl sheet beam vertically through the plume at the indicated times after laser ablation. Light from the bright plasma dominates for $\Delta t < 150$ µs. For $\Delta t = 200$-400 µs, the plasma luminescence extinguishes and two regions of clusters are observed. For $\Delta t > 500$ µs, surviving nanoparticles are observed on the front of the expanding plume. (b) Series of images as above compare spatial distributions of (top panel) Rayleigh scattering (308-nm light, scattered at 90°) from the top half of the plume [see dashed-line box] (middle panel) long-lived laser-induced photoluminescence, and (lower panel) residual plasma luminescence, which is approximately 1/10 as intense as the laser-induced luminescence. The brightest luminescence comes from the core of the plume, from clusters which are too small to scatter significant light by Rayleigh scattering (measured 1-10 nm as collected on the TEM grid at the position in (a) above)

EXPERIMENTAL RESULTS AND DISCUSSION

Polished *c*-Si wafers or zinc targets were ablated by KrF-laser pulses ($\lambda = 248$ nm, focused to energy densities of 5–8 J/cm² in 28-ns FWHM pulses) inside a large, turbopumped vacuum chamber (1×10^{-6} Torr base pressure) maintained at 1–15 Torr with pure (or mixtures of) 99.9999 % He , 99.9995 % Ar, 99.99% O_2 with variable flow controllers (0–1000 sccm).

After laser ablation,typical laser plasmas emit bright recombination luminescence from excited atoms and molecules which can be photographed at different time delays with the ICCD camera system (5 ns – 3 µs exposures). Figure 1(a) shows a minimal sequence of these digital photographs for the laser ablation of silicon into flowing He at 10 Torr. Within $\Delta t = 20$ µs, collisions with the background gas rapidly decelerate the plume of silicon vapor from an initial velocity of 2 cm/µs (kinetic energy/atom = 58 eV) to only 0.01 cm/µs (0.0015 eV).

To investigate Rayleigh scattering (RS) and photoluminescence (PL) from clusters suspended in the gas phase, a sheet of light from another pulsed laser (XeCl, $\lambda = 308$ nm, $h\nu = 4.0$ eV, 30 ns FWHM pulse, ~ 0.2 J/cm²) illuminated a 1.5-mm-wide cross section of the silicon plume from below.[12] Probe laser light scattered by nanoparticles (with estimated diameters larger than 2 nm)[13] was imaged by gating the camera on *during* the XeCl laser pulse. Alternatively, the camera was gated on *after* the probe laser pulse to capture images of long-lived PL.

In Fig. 1(a) the laser-induced PL is imaged along with the plasma recombination lumines-

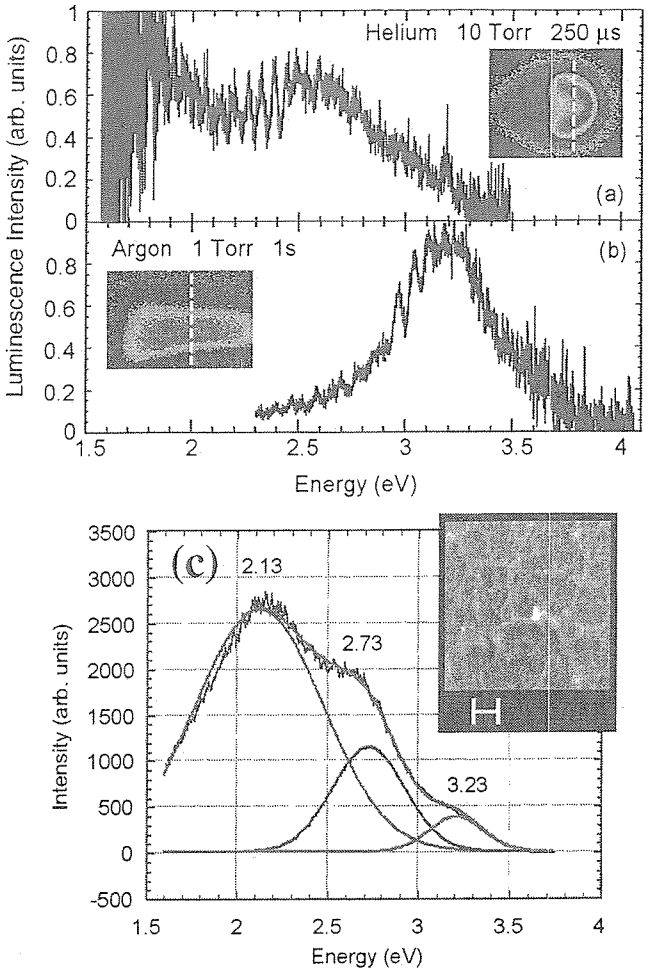

Fig. 2 - (a,b) Gated photoluminescence spectra from XeCl-laser-excited, gas-suspended nanoparticles 2-cm away from a laser-ablated Si target in (a) 10 Torr Helium, 250 µs after the ablation laser, and (b) 1 Torr argon, 1 second delay. Ten-shot averaged spectra, 2.6-nm resolution, 3-µs gate (starting 50-ns after the XeCl excitation pulse) using a gated-intensified diode array (Princeton Inst.) on a 0.3-m monochromator (Acton VM-503, 600 grooves/mm grating). In this case, the sheet of XeCl-light was turned parallel to the target surface.
(c) Strong RT PL spectra (CW, 325 nm, He-Cd laser excitation) from a weblike aggregate nanoparticle film (see inset) prepared in 1-Torr Ar/5%-O_2, collected on L-N_2 cooled Si substrate, and annealed at 800°C in O_2 (no PL) and then 1000°C for 30-min in Ar/5%-H_2 gas. *[spectrum courtesy of T. Makimura group, Univ. of Tsukuba]*

cence (which rapidly drops during the first 400 µs after ablation). By comparing images with and without the excitation pulse in Fig. 1(a), the laser-induced PL could be first discerned at Δt = 150–200 µs, near the front of the expanding plume. As shown in Figure 1(b), during Δt = 300–500 µs, the intensity of RS and PL increases at the front of the plume while a central core luminescence suddenly appears as the brightest region of PL in the images at Δt = 300 µs, and then collapses to the center of the plume, following the extinguishing core of plasma luminescence. This central core of bright luminescence originates from particles smaller than our RS detection threshold (determined by particle collection to be ~ 2 nm diameter), i.e. clusters. The 200 µs onset measured for the appearance of these clusters agrees with laser-induced fluorescence measurements which determined a 200 µs onset for silicon dimerization during ablation into 5 Torr He by Muramoto et al.[11]

For times > 0.5 ms, the nanoparticles segregate into a forward-going (v ~ 10 m/s), rotating ring, resembling a 'smoke ring' with a weak central trail of nanoparticles also visible. These dynamics, and the completely different dynamics resulting in a relatively uniform and stationary cloud of nanoparticles following ablation into heavier argon, are detailed in Ref. 12.

Three broad PL bands (at 1.8, 2.6, and 3.2 eV) were measured for gas-suspended nanoparticles generated by both Si/He and Si/Ar ablation. In general, the three bands occur simultaneously with similar measured decay lifetimes of ~ 1.8 µs.[12] These bands agree with those observed for oxidized *nc*-Si films and porous silicon.[15] The violet band is clearly linked to the presence of trace impurities of oxygen (from EELS analysis, see below) in the chamber, from the target, or in the ultrahigh purity gases used. This violet luminescence could be maximized by adjusting the flow of gas in the chamber (for Si/Ar, thereby controlling the mixing of the stationary nanoparticle cloud with oxygen-laden gas).[13] In argon, small admixtures of oxygen in the gas flow quenched the violet PL, as did stopping the flow. The maximally luminescent SiO_x stoichiometry was investigated by HREELS (see below). In helium, the turbulent dynamics resulted in

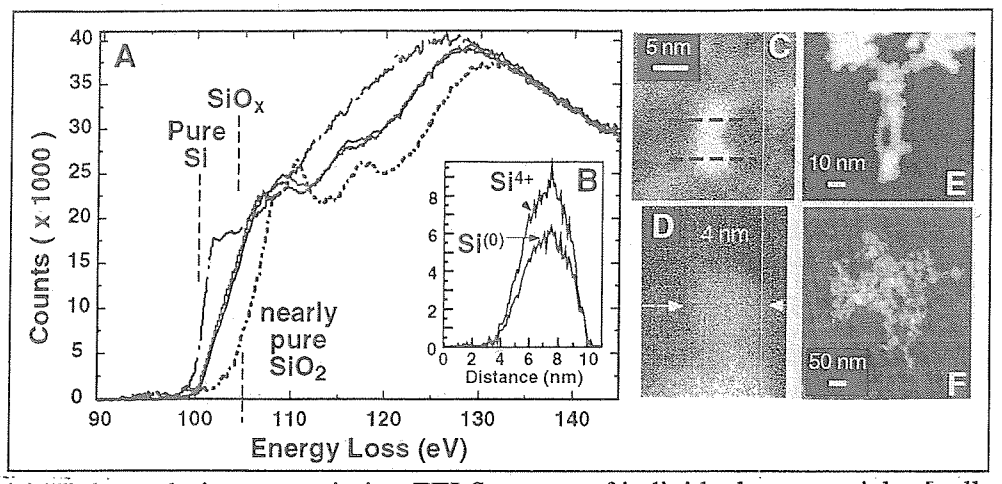

Fig.3 - (a) High-resolution transmission-EELS spectra of individual nanoparticles [collected on TEM grids as in Fig. 1(a)], and imaged by Z-contrast TEM, show a variation of stoichiometries ranging from pure silicon to nearly-pure SiO_2. (b) Translating the 0.27-nm electron beam across individual nanoparticles (as indicated in (c)) revealed that both the pure-silicon ($Si^{(0)}$) and pure-SiO_2 (Si^{4+}) regions are uniformly distributed throughout the 5-nm particles. Z-contrast TEM images showed 1–10 nm particles (c) aggregated in pairs, or (d) single particles for collection early in the expansion as in Fig. 1(a), or aggregated into (e) three-dimensional structures and (f) large networks of ~ 100–200 nm size for collection after many laser shots.

oxidation (and the growth of violet luminescence) for times > 300 μs after ablation, regardless of flow. However, the red and blue-green bands of luminescence appear together early in the expansion, and did not correlate with the extent of oxidation. Figure 2(a) shows these 1.8 and 2.6 eV PL bands measured at 250 μs. Some nearly-pure Si nanoparticles were collected on TEM grids placed at distances from the target which corresponded to the red and blue-green bands (as indicated for the position of the TEM grid in Fig. 1(a)).

This luminescence disappeared after deposition. Weblike films consisting of these aggregated nanoparticles required standard passivation and annealing to exhibit RT PL (Fig. 2(c)). Similar bands (slightly red-shifted red 2.1 eV, blue-green 2.7 eV, and violet 3.2 eV) were retained .

The high-resolution PL-spectra of Fig. 2 reveal a pronounced oscillatory structure decorating the low-energy sides of each of the three PL bands from the gas-suspended nanoparticles. This structure was reproducible at different time delays. In fact, the entire spectrum could be deconvoluted as a sum of Gaussian lineshapes.[13] For the 3.2 eV band in Fig. 2(b), the spacing is quite uniform (62 ± 6 meV) across the spectral region. This roughly agrees with the spacing observed for the 2.6 eV band of Fig. 2(a) (57 ± 5 meV). The 1.8 eV band appeared to contain an additional vibronic series (only an average interpeak spacing of 34 ± 6 meV was derived).[13]

Numerous reports of both irregular and regular spectral features decorating PL from *nc*-Si and *P*-Si are reviewed in Ref. 13. However, the most likely explanation for the regular vibronic structure in Fig. 3 is photoexcitation of Si-Si vibrations at localized surface states, or from unassigned transitions in highly vibrationally-excited Si_2 which is weakly bound or photodissociated from the nanoparticle surface. In support of surface state luminescence, Kimura and Iwasaki recently reported clear vibronic structure decorating broad ultraviolet and blue PL bands from isolated (4–10 nm) silicon nanocrystals suspended in organic liquids at room temperature. Unlike the apparent Si-Si vibronic modes in our measurements, Si-O-Si and other modes were found, indicating that the vibronic fine structure originated from a localized surface state.[16] Orii et al recently observed similar vibronic luminescence with increasing fluence during PL in the CdSe nanocrystal system which they attributed to photodissociated Se_2 dimers.[17]

For *c*-Si ablation into 1 Torr Ar or 10 Torr He, spherical 5 nm diameter nanoparticles were collected (2 cm from the target) with other sizes ranging from 1–10 nm. For deposits collected after 1–10 laser shots, individual and or small groups of nanoparticles (as in Fig. 3(c,d)) were found. For deposits collected after hundreds of laser shots, groups of ~ 5 nm particles were also

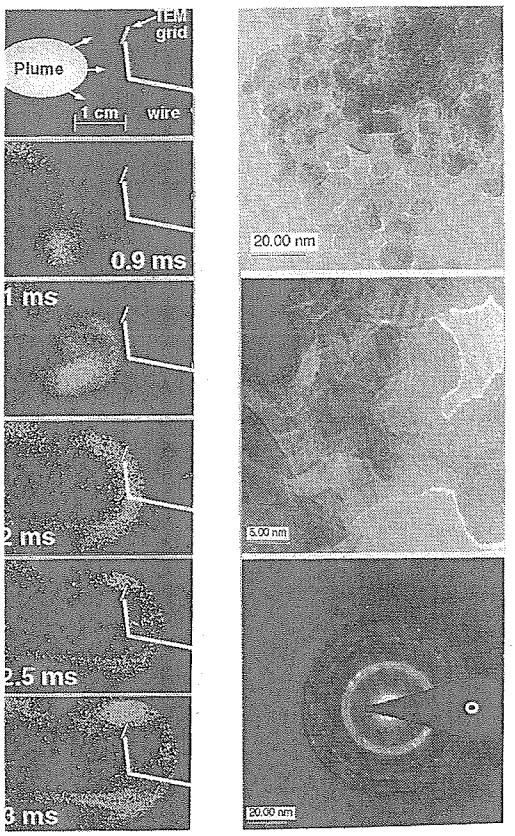

Fig.4 - **(left)** Gated-ICCD-photographs of XeCl-laser induced luminescence from 5-20 nm ZnO nanoparticles formed when a 2"-target of Zn metal (left of frame) is KrF-laser-ablated into a 7.5 Torr Ar/O_2 mixture (5 Torr Ar / 2.5 Torr O_2). The position of the TEM collection grid is shown in the images. These PL images (and RS images, not shown) indicate that clusters of 5–20 nm size require 1–3 ms to grow. **(right)** Bright field TEM images and electron diffraction patterns reveal crystalline ZnO nanoparticles, 5–20 nm in size, of hexagonal zincite.

found in aggregates of up to 100–300 nm dimensions (Figs. 3(e,f)). These aggregates interlinked to form a web-like microstructure very similar to those reported by El-Shall *et al.*[4] Individual nanoparticles were examined for composition and nanostructure with HREELS (0.27 nm spatial resolution, energy resolution ~ 0.8 eV). The intensity and ELNES (energy loss near edge structure) were examined at the Si-L absorption edge in Si (99 eV) and SiO_2 (102 eV), and at the O–K absorption edge to determine the nanoparticle composition. As shown in Fig. 3(a), particles were found with stoichiometries between nearly-pure Si to nearly-pure SiO_2.

Compositional profiles of individual SiO_x nanoparticles were acquired by translating the STEM beam (as indicated in Fig. 3(c)) while ~100 ELNES spectra were recorded. These HREELS linescans showed (as in Fig. 3(b)) a uniform distribution of $Si^{(0)}$ bonding (as in pure silicon) and $Si^{(4+)}$ bonding (as in pure SiO_2). The particles appear to be composed of a homogeneous mixture of pure and oxidized Si regions, which contrasts with surface-oxidized Si nanoparticles produced and analyzed in other studies.[1] Although the TEM resolution was sufficient to resolve lattice fringes from *c*-Si by Z-contrast imaging, repeated attempts were unsuccessful, indicating either amorphous silicon or *c*-Si regions in the sub-1 nm size range (i.e. clusters of *c*-Si < 25 atoms).

The *ex situ* stability of as-deposited nearly-pure silicon nanoparticles indicates that oxidation leading to the overall stoichiometry is accomplished in the gas phase. In all cases where violet gas phase PL was observed, SRSO nanoparticles were collected. Introduction of oxygen-containing impurities (oxygen, water vapor) to condensing Si nanoparticles was controlled by increasing the Ar flow. This condition correlated with an overall *ex situ* $SiO_{1.4}$ stoichiometry.

These same techniques have now been applied for the growth of crystalline Ge, SiGe, ZnO, Y_2O_3, and MgO nanoparticles. Figure 4 shows laser-induced luminescence images which trace the appearance, growth, and propagation of ZnO nanoparticles following KrF laser ablation of Zn metal into a 7.5 Torr Ar/O_2 mixture. Direct imaging of the particle collection process shows that particles were collected on the TEM grid from 2–3 ms after ablation. After 20 laser shots, ex situ bright-field TEM images and electron diffraction measurements shown in Figure 4 reveal that

aggregated 5–20 nm diameter hexagonal zincite ZnO nanocrystals were formed.

CONCLUSIONS

In situ imaging of PL and RS from nanoparticles formed by laser ablation into background gases reveals long times for nanoparticle growth (Si: $\Delta t = 3$ ms in 1 Torr Ar, $\Delta t = 200$ μs in 10 Torr He, ZnO: 1-3 ms in 7.5 Torr Ar/O_2). In situ PL spectroscopy of Si nanoparticles reveals a changing spectrum, with the additional 3.2 eV band appearing and growing to dominate the 1.8 eV and 2.6 eV bands according to the extent of oxidation in the plume (as analyzed by ex situ HREELS and ELNES). Maximal violet PL correlated to a $SiO_{1.4}$ stoichiometry in nanoparticles of uniform composition. The brightest gas-phase PL for Si/He in Figs. 1, 2(a) correlated to clusters too small to detect by RS (< 2 nm). The size-independence of the broad PL spectra and apparent vibronic structure, coupled with the measured distribution of particle sizes, suggest a surface luminescence origin. Nanoparticle-aggregate films were deposited which required standard passivation annealing before bright photoluminescence could be obtained. The film PL exhibited bands similar to the gas-suspended nanoparticles, but without vibronic structure. The fact that SiO_x nanoparticles, when isolated in the background gas, did show strong luminescence demonstrates the critical role of isolation.[18] Oxidation of nanocrystals is necessary as a means of isolation in thin films, however partial oxidation accompanied by spatial isolation in the gas phase appears to produce the same result. Crystalline ZnO nanoparticles (< 20 nm) were similarly detected following formation in 7.5 Torr Ar/O_2 and deposited 1-3 ms following laser ablation of Zn metal. The authors gratefully acknowledge valuable research assistance by T. Makimura, C.W. White and B.C. Sales. This research was sponsored by the Oak Ridge National Laboratory, managed by Lockheed Martin Energy Research Corp., for the U.S. Department of Energy, under contract DE-AC05-96OR22464.

REFERENCES

1. W. L. Wilson, P. F. Szajowski, L.E. Brus, *Science* **262**, 1242 (1993).
2. S. Schuppler, S. L. Friedman, M. A. Marcus, D. L. Adler, Y.-H. Xie, F. M. Ross, Y. J. Chabal, T. D. Harris, L.E. Brus, W.L. Brown, E. E. Chaban, P. F. Szajowski, S. B. Christman, and P. H. Citrin, *Phys. Rev. B* **52**, 4910 (1995).
3. (a) L.A. Chiu, A. A. Seraphin, and K.D. Kolenbrander, *J. Electronic Materials* **23**, 347 (1994). (b) E. Werwa, A. A. Seraphin, L.A. Chiu, C. Zhou, and K.D. Kolenbrander, *Appl. Phys. Lett.* **64**, 1821 (1994).
4. (a) M.S. El-Shall, S. Li, and T. Turkki, D. Graiver, U.C. Pernisz, M.I. Baraton, *J.Phys. Chem.* **99**, 17805 (1995). (b) S. Li, S.J. Silvers, and M. S. El-Shall, *J. Phys. Chem. B*, **101**, 1794 (1997).
5. I.A. Movtchan, W. Marine, R.W. Dreyfus, H.C. Le, M. Sentis, and M. Autric, *Appl. Surf. Sci.* **96-98**, 251 (1996).
6. (a) T. Yoshida, S. Takeyama, Y. Yamada, and K. Mutoh, *Appl. Phys. Lett.* **68**, 1772 (1996). (b) Y. Yamada, T. Orii, I. Umezu, S. Takeyama and T. Yoshida, *Jpn. J. Appl. Phys.* **35**, 1361 (1996).
7. T. Makimura, Y. Kunii, and K. Murakami, *Jpn. J. Appl. Phys.*, **35** 4780 (1996).
8. (a) *Pulsed Laser Deposition of Thin Films,* Ed. by D. B. Chrisey and G. K. Hubler, (Wiley-Interscience Pub lisher), 1994., (b) D.H. Lowndes, D. B. Geohegan, A. A. Puretzky, D. P. Norton, and C.M. Rouleau, *Science* **273**, 898 (1996).
9. T. Yoshida, Y. Yamada, and T. Orii, *Technical Digest of the International Electron Devices Meeting*, San Fran cisco, CA, Dec. 8-11, 1996, IEEE.
10. K.D. Hirschman, L. Tsybeskov, S.P. Duttagupta, and P.M. Fauchet, *Nature* **384**, 338 (1996).
11. J. Muramoto, Y. Nakata, T. Okada and M. Maeda, *Jpn. J. Appl. Phys.* **36** L563 (1997).
12. D. B. Geohegan, A. A. Puretzky, G. Duscher, and S. J. Pennycook, *Appl. Phys. Lett.* **72**, 2987 (1998) and references cited therein..
13. D. B. Geohegan, A. A. Puretzky, G. Duscher, and S. J. Pennycook, *Appl. Phys. Lett.* **73**, 438 (1998) and references cited therein.
14. H.C. van de Hulst: *Light Scattering by Small Particles* (Dover Publications, New York, 1981).
15. Broad reviews are given by (a) P. M. Fauchet, *J. Lumin.* **70**, 294 (1996). (b) F. Koch, V. Petrova-Koch, *J. Non-Cryst. Solids* **198-200**, 846 (1996).
16. K. Kimura and S. Iwasaki, *Mat. Res. Soc. Proc.*, **452**, 165 (1997).
17. T. Orii, S. Kaito, K. Matsuishi, S. Onari, and T. Arai, J. Phys. D: Condesn. Matter **9**, 4483 (1997).
18. Louis Brus, *J. Phys. Chem.* **98**, 3575 (1994.